Double giant dipole resonance in the (π^-, π^+) reaction

H. Ward, K. Johnson, G. Kahrimanis, D. Saunders, and C. Fred Moore
University of Texas at Austin, Austin, Texas 78712

S. Mordechai
Ben-Gurion University of the Negev, Beer-Sheva 84105, Israel
and University of Texas at Austin, Austin, Texas 78712

C. L. Morris
Los Alamos National Laboratory, Los Alamos, New Mexico 87545

H. T. Fortune, M. A. Kagarlis, D. A. Smith, and J. M. O'Donnell*
University of Pennsylvania, Philadelphia, Pennsylvania 19104

N. Auerbach†
Los Alamos National Laboratory, Los Alamos, New Mexico 87545
and University of Pennsylvania, Philadelphia, Pennsylvania 19104

The double isovector giant dipole state has been observed in the (π^-, π^+) $\Delta T_z = +2$ double-charge-exchange reaction on ^{13}C, ^{27}Al, ^{40}Ca, ^{56}Fe, ^{59}Co, and ^{93}Nb. The resonances observed in the (π^-, π^+) reaction are closely related via Coulomb displacement energy and isospin symmetry to the resonances measured in the inverse (π^+, π^-) reaction on the same nuclei. The new observations provide a direct determination of the upper isospin component of the double giant dipole state, which is generally very weak in the (π^+, π^-) reaction. The comparison between the double dipole in the two double-charge-exchange modes gives valuable information on the isospin splitting and the Pauli-blocking effects for isotensor transitions.

PACS number(s): 25.80Gn, 21.10.Re

I. INTRODUCTION

In a recent paper [1] we reported the first observation of a double-isovector giant-dipole resonance in nuclei in the (π^+, π^-) double-charge-exchange (DCX) reaction on ^{nat}S. More recent data [2, 3] clearly show the existence of these exotic resonances in the continuum at high excitation energies. The identification of the double-dipole resonances is based on their centroid energies, characteristic angular distributions, cross sections, and comparison with the inverse DCX reaction [2, 3]. Pion DCX offers a cleaner way to study double giant resonances than that offered by inelastic reactions because of the selectivity of the DCX reaction and the clear geometrical signature of the angular distributions of the various giant resonances (GR) due to the strong absorption of the pions. An additional unique feature of pion DCX used in this study is the simplicity with which one can study the inverse reaction. There are four advantages to measuring the double-dipole resonance in the (π^-, π^+) reaction: (a) The double dipole is expected to appear at a significantly lower energy and with a lower background level from the continuum than in the (π^+, π^-) mode. The decrease in energy of the double dipole in the (π^-, π^+) reaction is about four Coulomb energies (after correcting for the symmetry energy and the neutron-proton mass difference), and that is a significant shift for medium and heavy nuclei. For example, the double dipole is observed at $Q = -49.9$ MeV ($E_x = 47.3$ MeV in ^{93}Tc) in ^{93}Nb$(\pi^+, \pi^-)^{93}$Tc, but (as we see below) in the inverse reaction it appears at $Q = -24.9$ MeV ($E_x = 20.9$ MeV in ^{93}Y). (b) In (π^-, π^+) the spectra should be simpler because the double isobaric analog state (DIAS) and the giant dipole built on the isobaric analog state (GDR⊗IAS) resonances do not exist, and therefore the double dipole is the lowest resonance expected in the reaction. (c) The double dipole is expected to have a smaller width in (π^-, π^+) than in the inverse reaction. (d) The double GDR reached in (π^-, π^+) has a single isospin component, as will be discussed later. We note, however, that measurements of (π^-, π^+) are much more difficult than (π^+, π^-), because π^+ beam fluxes are generally larger by about a factor of 6 relative to the π^- fluxes at the energies of interest for the present study. Furthermore, for all $N > Z$ nuclei the cross sections for the double dipole in (π^-, π^+) are smaller than those in (π^+, π^-) because of the Pauli-blocking effect, making the running time for a single measurement significantly longer.

---

*Present address: Los Alamos National Laboratory, Los Alamos, New Mexico 87545.
†Permanent address: Tel-Aviv University, Tel-Aviv, Israel.

TABLE I. Target compositions, areal densities, and angles of measured data points.

Target	Isotopic purity (%)	Areal density (g/cm^2)	Scattering angles (lab)
^{13}C	90.0	0.329	5°
^{27}Al	100.0	1.713	5°
^{40}Ca	96.9	2.38	5°, 12°, 19°
^{56}Fe	91.8	2.44	5°
^{59}Co	100	1.079	5°
^{93}Nb	100	3.428	5°

II. EXPERIMENT

The measurements were performed with the energetic pion channel and spectrometer (EPICS) at Clinton P. Anderson Meson Physics Facility (LAMPF) with the standard pion double-charge-exchange setup [4]. Table I lists the pertinent information on the targets and on the measured data points, all of which were at $T_\pi =$ 295 MeV. Electrons were eliminated using an isobutane velocity-threshold Cherenkov detector in the focal plane. A scintillator placed behind a series of aluminum and graphite wedges was used to detect and veto muon events [5]. The remaining background was pions resulting from continuum DCX in the target. The choice of the highest beam energy available at EPICS ($T_\pi =$ 295 MeV) for the present measurements has several advantages: (a) the background level from the continuum is lower since the excitation-energy region of interest is away from the inclusive DCX peak, (b) a larger outgoing energy range ($\approx$ 50 MeV) is covered by the acceptance of the spectrometer in a single setting, (c) cross sections are expected to increase as k^2 or faster, where k is the incident pion momentum, and (d) the highest energy was chosen because it is here that sequential processes dominate DCX. This is evidenced by the dominance of the excitation of the DIAS at $\theta = 5°$.

The acceptance of the spectrometer was measured with a ^{12}C target using inelastic scattering to the 4.44-MeV state at an energy $T_\pi =$ 180 MeV and a scattering angle of 35°, which corresponds to the peak cross section. The spectrometer field was varied to move the 4.44-MeV peak across the focal plane, covering approximately ±10% of the central momentum of the spectrometer. Absolute normalization was obtained using a polyethylene (CH$_2$) target of areal density 0.068 g/cm^2 to measure the hydrogen elastic cross section and comparing the yields with cross sections calculated from π-nucleon phase shifts [6].

III. RESULTS AND ANALYSIS

A. Discussion of the data

Figure 1 presents the ^{13}C(π^-, π^+)^{13}Be and the previous ^{13}C(π^+, π^-)^{13}O Q-value spectra measured under the same experimental conditions at $\theta_{lab} =$ 5° and incoming pion energy $T_\pi =$ 295 MeV. The spectra have been

corrected for the spectrometer acceptance as a function of momentum. The (π^-, π^+) data are from the present measurement and the (π^+, π^-) fit results from reanalysis of recent data from Ref. [2]. In addition to the weak transitions to the ground states of ^{13}Be and ^{13}O, respectively, both spectra contain a wide peak labeled (GDR)^2 located high in the continuum region. In the (π^+, π^-) reaction the resonance is observed [2] at $Q = -46.5$ MeV, but in the inverse reaction, (π^-, π^+), the resonance appears around $Q = -49.5$ MeV. The energy relation between the two DCX modes is discussed in Sec. II B. The giant resonance (GR) peaks were fitted with a Lorentzian shape of variable width. The fits in Fig. 1 use Γ(GDR^2) $= 9.0$ MeV for (π^-, π^+) and 12.0 MeV for (π^+, π^-). Figure 1(a) demonstrates also the existence of three low-lying states below the g.s. of ^{13}Be. These weak transitions arise from the 10% ^{12}C impurity in the ^{13}C target (Table I) and correspond to the g.s. and two excited states at 2.1 and 4.6 MeV in ^{12}Be. In (π^+, π^-) the corresponding states of ^{12}O are also present. They lie between the GDR$\otimes$IAS and the (GDR)^2 in Fig. 1(b). The backgrounds (dashed lines) which arise from the DCX cross section to the continuum were fitted using a third-order polynomial function of the Q value: background(Q, θ) $=$ $a_0(\theta) + a_1(\theta)Q + a_2(\theta)Q^2 + a_3(\theta)Q^3$, where Q is the absolute Q value. The same background form was used for both DCX modes. The solid lines are the resulting
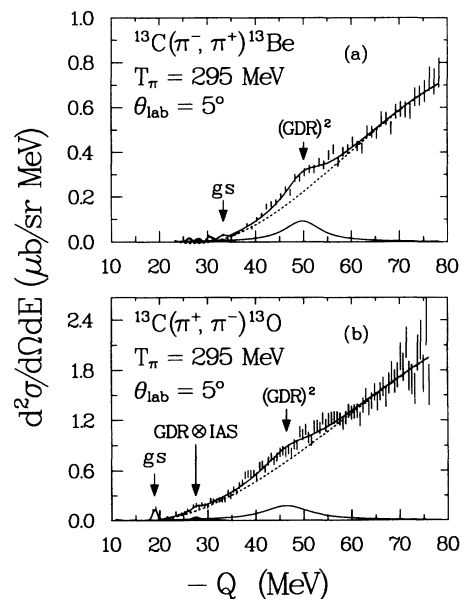

FIG. 1. (a) Doubly differential cross-section spectrum for the ^{13}C(π^-, π^+)^{13}Be reaction at $T_\pi =$ 295 MeV and $\theta_{lab} =$ 5°. The arrows indicate the fitted location of the ground state (g.s.) and the giant resonance (GDR)^2. Short vertical lines represent statistical uncertainty of the data. The dashed line is the background fitted with a polynomial shape and the solid line is the fit to the spectrum using NEWFIT. (b) Same as (a) except for the ^{13}C(π^+, π^-)^{13}O reaction. The arrows indicate the fitted location of the g.s., the giant dipole built on the isobaric analog state (GDR$\otimes$IAS), and the double giant dipole (GDR^2).

TABLE II. Double-dipole Q values for the (π^-, π^+) reaction extracted from the present study compared with previous data from the (π^+, π^-) reaction [2] measured on the same target nuclei.

Target	(π^+, π^-)		(π^-, π^+)	
	$Q_{g.s.}$ [a] (MeV)	Q_{DD} (MeV)	$Q_{g.s.}$ [a] (MeV)	Q_{DD} (MeV)
^{13}C	-18.96	-46.5 ± 2.0	-32.84	-49.5 ± 0.5
^{27}Al	-15.42	-49.1 ± 0.5	-12.57	-36.2 ± 0.3
^{40}Ca	-24.76	-54.0 ± 0.5	-0.83	-31.1 ± 0.3
^{56}Fe	-5.68	-54.4 ± 0.6	-6.33	-31.0 ± 1.0 [b]
^{59}Co	-4.85	-48.6 ± 0.8	-7.77	-35.0 ± 0.5
^{93}Nb	-2.58	-49.9 ± 0.8	-3.99	-24.9 ± 1.0

[a] Values from the 1986 mass table [24].

[b] A new measurement of the (π^-, π^+) reaction on ^{56}Fe (including the elastic offset in the DCX data) gives $Q_{DD} = -31.0$ MeV rather than -33.8 MeV reported in Ref. [2].

FIG. 2. Same as Fig. 1 except for ^{59}Co target.

fits to the spectra. The resonance labeled $(GDR)^2$ in the (π^+, π^-) reaction was previously [2] identified as the double isovector giant-dipole resonance. The strengths of the double dipoles reached in the (π^-, π^+) reactions and the ratios $\sigma_{DD}(\pi^-, \pi^+)/\sigma_{DD}(\pi^+, \pi^-)$ will be discussed later. The lower GR observed in the (π^+, π^-) spectrum was identified [7] as the giant dipole built on the isobaric analog state and is labeled GDR⊗IAS in Fig. 1(b). This resonance is very weak at $5°$ but appears very clearly at $\theta_{lab} = 18°$, an angle which corresponds to the peak of the dipole angular distribution at this energy [8]. The resonance is absent in the (π^-, π^+) spectrum, because no transition to the isobaric analog state (IAS) is allowed in this reaction mode. The computer program NEWFIT [9] was used to fit the spectra in these figures and to extract the parameters listed in Tables II and III.

Figure 2 displays the (π^-, π^+) and (π^+, π^-) Q-value spectra on ^{59}Co. For $T \geq 2$ nuclei the double dipole in the (π^+, π^-) reaction splits into five isospin components. However, in (π^-, π^+), isospin considerations limit the reaction to only the upper isospin component $(T_> = T+2)$. These states are illustrated schematically in Fig. 3. Sim-
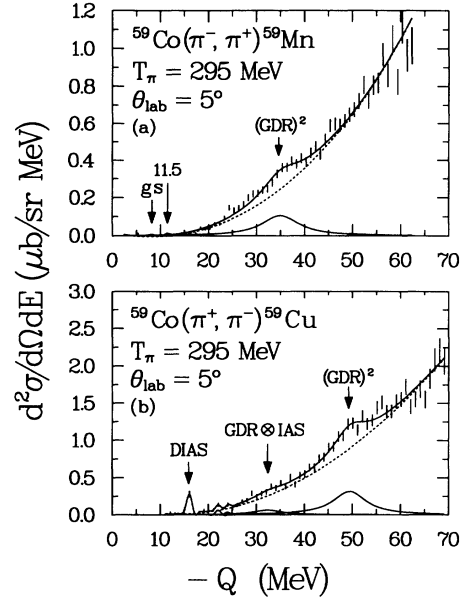
ple double-isospin coupling arguments give the strength ratios listed in the figure as $(\sum C_1 C_2)^2$. Pauli-blocking effects will further suppress the upper isospin members of the double dipole in ^{59}Cu. Therefore the observed resonance in the (π^+, π^-) reaction [Fig. 2(b)] contains mainly the three unresolved lower isospin components, whereas the double dipole in the (π^-, π^+) reaction [Fig. 2(a)] has only a single $(T = 9/2)$ isospin component. An additional obvious difference between the spectra in Fig. 2 is the presence of the DIAS and the GDR⊗IAS transitions in the (π^+, π^-) spectrum. Both transitions are absent in the (π^-, π^+) mode. The spectra measured on the other targets are quite similar to those presented in Figs. 1 and 2 and are not shown here. The measured Q values for the double dipole are given in Table II. Table III gives all the measured quantities for the double GDR (Q values, cross sections at $5°$ and the widths) for both reaction modes. Also listed in Table III are the ratios of the double-dipole cross sections in (π^-, π^+) and

TABLE III. Results from the (π^+, π^-) and (π^-, π^+) double-charge-exchange reactions on ^{13}C, ^{27}Al, ^{40}Ca, ^{56}Fe, ^{59}Co, and ^{93}Nb at $T_\pi = 295$ MeV and $\theta_{lab} = 5°$.

Target	(π^+, π^-) [a]			(π^-, π^+) [b]			$\dfrac{\sigma_{DD}(\pi^-, \pi^+)}{\sigma_{DD}(\pi^+, \pi^-)}$	ΔE_C [c]	$\Delta E_S'$ [d]
	$-Q_{DD}$ (MeV)	$(d\sigma/d\Omega)_{DD}$ (μb/sr)	Γ (MeV)	$-Q_{DD}$ (MeV)	$(d\sigma/d\Omega)_{DD}$ (μb/sr)	Γ (MeV)		(MeV)	(MeV)
^{13}C	46.5 ± 2.0	3.2 ± 0.5	12.0 ± 3.0	49.5 ± 0.5	1.3 ± 0.2	9.0 ± 1.4	0.41 ± 0.09	2.71	8.7 ± 2.0
^{27}Al	49.1 ± 0.5	2.4 ± 0.2	8.4 ± 2.0	36.2 ± 0.3	0.95 ± 0.09	6.4 ± 1.0	0.40 ± 0.05	5.19	2.7 ± 0.6
^{40}Ca	54.0 ± 0.5	2.6 ± 0.2	9.0 ± 1.4	31.1 ± 0.3	3.2 ± 0.2	9.0 ± 1.0	1.23 ± 0.12	7.30	1.13 ± 0.6
^{56}Fe	54.4 ± 0.6	3.1 ± 0.3	10.0 ± 1.5	31.0 ± 1.0	1.2 ± 0.1	10.0 ± 1.6	0.39 ± 0.05	8.74	5.7 ± 1.2
^{59}Co	48.6 ± 0.8	4.1 ± 0.8	8.2 ± 2.0	35.0 ± 0.5	1.5 ± 0.2	9.2 ± 1.4	0.37 ± 0.09	8.90	17.0 ± 0.9
^{93}Nb	49.9 ± 0.8	3.5 ± 0.5	8.8 ± 2.6	24.9 ± 1.0	0.8 ± 0.3	8.5 ± 2.0	0.23 ± 0.09	11.9	17.4 ± 1.3

[a] Reference [2], except for the ^{27}Al data which is taken from Ref. [3].

[b] Present data.

[c] Sources for the Coulomb energy values are described in the text.

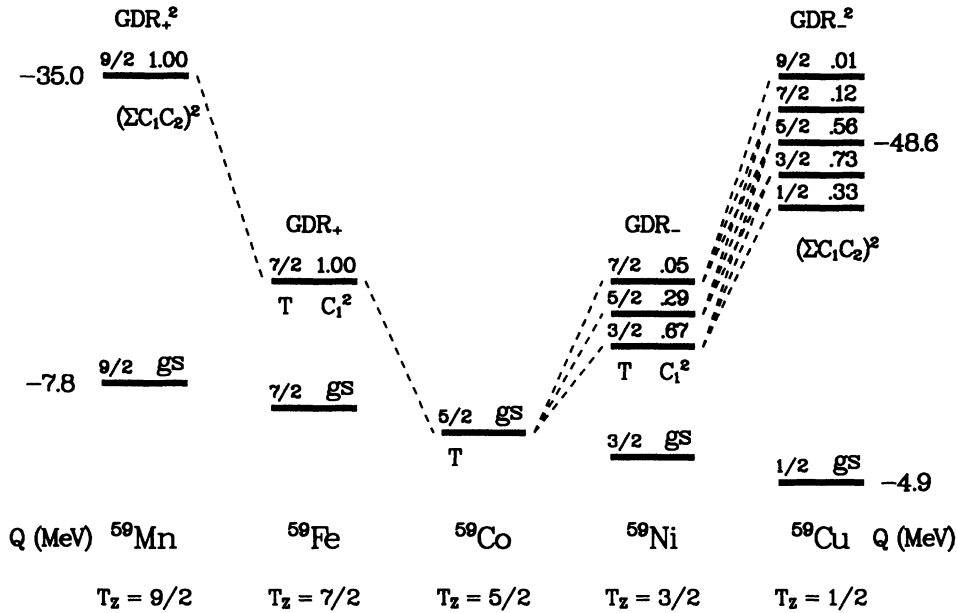[d] $\Delta E_S' = Q_{DD}(\pi^+, \pi^-) - Q_{DD}(\pi^-, \pi^+) - 4(\Delta E_C - \Delta m_{np})$.

FIG. 3. Level scheme for DCX to the double isovector giant-dipole resonances on ^{59}Co. Vertical placement of states is not to scale. C_1 and C_2 are isospin Clebsch-Gordan coefficients, and the sums indicate double coupling coefficients. The listed Q values on the right and left sides are from previous [2] and present experiments.

(π^+, π^-), the Coulomb displacement energies, and the energy differences $\Delta E'_S$ discussed later.

B. Energy relations and symmetry energy

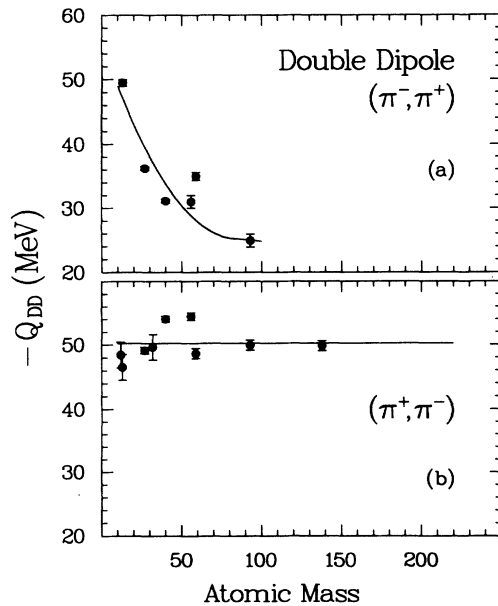Figure 4 displays the observed Q value for the double dipole as a function of atomic mass. In (π^+, π^-) the dou-

FIG. 4. Q values versus A for the double dipole in both pion DCX modes. (a) (π^-, π^+) data from the present study. The curve is to guide the eye. (b) (π^+, π^-) data from Ref. [2]. The solid line is the least-mean-square value.

ble GDR appears around $Q = -50$ MeV and its energy is almost independent of A. The doubly excited GDR in the (π^+, π^-) reaction is reached by adding two $E1$ vibrational energies and two Coulomb energies to the target nucleus ground state. The $E1$ energy decreases with A, but the Coulomb energy increases with Z and the two effects almost cancel each other, yielding a nearly constant Q value for the double GDR excitations. Experimentally the single-charge-exchange GDR is observed in (π^+, π^0) around $Q = -25$ MeV for a wide range of mass. Thus the energies of the double dipoles observed in (π^+, π^-) are close to double the energy of the "single" GDR, i.e.,

$$Q_{(\pi^+, \pi^-)}(\text{GDR}^2) \simeq 2Q_{(\pi^+, \pi^0)}(\text{GDR}) \simeq -50 \text{ MeV}. \quad (1)$$

This near equality is surprising because it neglects the effect of isospin splitting, which exists in both the (π^+, π^0) and (π^+, π^-) reactions, but is somewhat different in the two. The double GDR observed in (π^-, π^+) [Fig. 4(a)] has a significantly different trend. This state is obtained by adding two $E1$ vibrational energies to the nucleus and subtracting two Coulomb energies, since two protons are changed into two neutrons. Thus the Q values in (π^-, π^+) are expected to decrease strongly (in absolute value) with A. The lowering of the magnitude of the double-dipole Q value is very significant for medium and heavy nuclei. For example, the double dipole on ^{93}Nb has $Q = -49.9$ MeV in ^{93}Nb$(\pi^+, \pi^-)^{93}$Tc but appears as low as $Q = -24.9$ MeV in the ^{93}Nb$(\pi^-, \pi^+)^{93}$Y reaction. The solid line drawn in Fig. 4(a) is merely to guide the eye while the line in Fig. 4(b) is a least-squares constant fit to the data which gives $Q = -50.2$ MeV, for $12 \leq A \leq 197$.

The energy relation between the double dipole in the two DCX modes can be written as

$$Q_{\mathrm{DD}}(\pi^-,\ \pi^+) - Q_{\mathrm{DD}}(\pi^+,\ \pi^-) = 4(\Delta E_C - \Delta m_{np}) - \Delta E_S' \tag{2}$$

where ΔE_C is the average Coulomb displacement energy for the $T_0 + 2$ multiplet with $T_z = (T_0 + 2)$, $(T_0 + 1)$, T_0, $(T_0 - 1)$, and $(T_0 - 2)$. The quantity Δm_{np} is the neutron-proton mass difference (1.29 MeV). Equation (2) then defines $\Delta E_S'$ which is related to the symmetry energy of the single GDR [10]. We have used experimental values for the $T_0 + 1$ multipole Coulomb displacement energies when the neighboring states in the multiplet are known (up to mass 40). For heavier nuclei, only one pair of states is known. In order to avoid odd-even mass difference ambiguities we have used the relation [11]

$$\Delta E_C = \frac{1.412Z}{A^{1/3}} - 0.861 \text{ MeV}, \tag{3}$$

where Z and A refer to the atomic and mass numbers, respectively, of the target nucleus. The Coulomb energies are listed in Table III.

Using Eq. (2) and the experimental Q values listed in Table III, we obtain the $\Delta E_S'$ values given in the table. These quantities give the energy differences between $T_>$ and the centroid of the double-dipole members reached in the $(\pi^+,\ \pi^-)$ reaction. For ^{13}C the $T_<$ and $T_>$ components of the GDR have been measured in photonuclear studies [12]. The centroids of the two components are separated by 6.8 MeV from which a Lane potential $[V = 6.8A/(T + 1)]$ of 59 MeV can be derived. This can then be used to calculate the expected line shape for the double dipole in $(\pi^+,\ \pi^-)$, following the procedures outlined in Ref. [10]. The 10% contribution from the upper isospin component causes the extracted value of $\Delta E_S'$ to shift to 8.7 ± 2.0 MeV. The value of $\Delta E_S'$ can be calculated knowing the Lane potential [10] giving an expected value of 10.3 MeV, which compares favorably with our measured value. Using the same Lane potential (59 MeV) we expect $\Delta E_S'$ for ^{27}Al to be 4.96 MeV, which compares with our extracted value of 2.7 ± 0.6 MeV. A discrepancy is also apparent in the $T = 0$ data. Here we expect $\Delta E_S' = 0$, but for ^{40}Ca we extract $\Delta E_S' = 1.13 \pm 0.6$ MeV, although here the deviation is in the other direction. These deviations are not currently understood, but may be related to a poor estimate of the Coulomb displacement energy, or the assumption that the Lane potential is the same for single and double resonances. For heavier nuclei the values of $\Delta E_S'$ for the doubly excited GDR deduced from Eq. (2) are expected to be much larger than for the single GDR since the states involved differ by several ($\approx$ three or more) isospin units as illustrated in Fig. 3, for the case of ^{59}Co.

C. Angular distribution of the double dipole

Figure 5 displays the angular distribution measured for the double dipole for both ^{40}Ca$(\pi^+,\ \pi^-)^{40}$Ti (from Ref. [2]) and ^{40}Ca$(\pi^-,\ \pi^+)^{40}$Ar. The figure contains data from the present work for the ^{40}Ca$(\pi^-,\ \pi^+)^{40}$Ti measurements at three laboratory scattering angles 5°, 12°, and 19°. Figure 5 shows that the new partial an-

gular distribution measured in $(\pi^-,\ \pi^+)$ is nearly identical to the angular distribution measured earlier under the same experimental conditions in the $(\pi^+,\ \pi^-)$ reaction. The dot-dashed lines are the results of simple sequential-model calculations using the pion coupled-channel impulse-approximation (CCIA) code NEWCHOP [13]. The calculations include the ground state (g.s.), the giant-dipole resonance (GDR), and the double dipole (GDR^2). The dashed lines are the calculations for the double dipole with $J^\pi = 2^+$ and the dotted lines are for $J^\pi = 0^+$. The solid lines are the sums of the 0^+ and 2^+ curves with the normalization factors listed in the figure. The normalization factors for the 0^+ curves were chosen to account for the forward-angle rises of the cross sections when added to the 2^+ curves. Both angular distributions show a forward-angle rise which may indicate a contribution of the $J^\pi = 0^+$ double-dipole state [14]. The small (but nonzero) normalization factors for the 0^+ curves indicate that the observed resonances are primarily the $J^\pi = 2^+$ double-dipole states, but may indicate
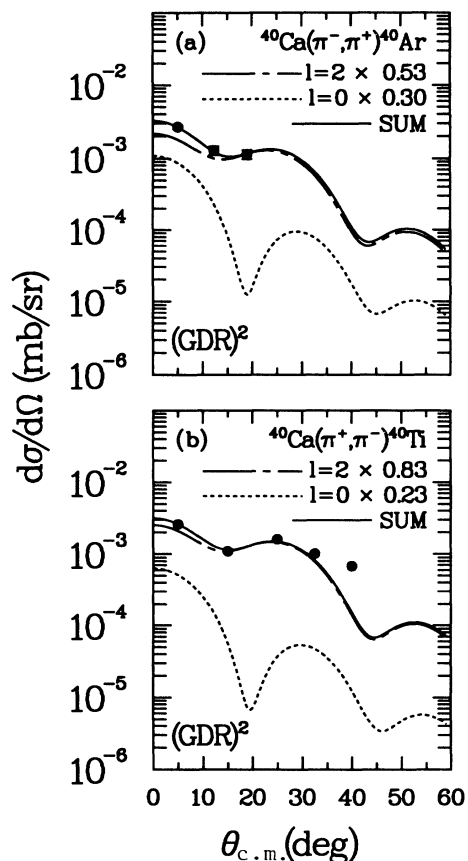
FIG. 5. Angular distributions for the resonances identified as the double dipoles in the ^{40}Ca$(\pi^\pm,\pi^\pm)$ reactions at $T_\pi = 295$ MeV. The curves are sequential-model calculations for the double dipole using NEWCHOP [13]. The dashed line is a 2^+ distribution normalized to fit the (a) 19° and (b) 15° data points. The dotted lines are 0^+ curves normalized such that the sum of the 2^+ and 0^+ distributions fits the forward-angle cross sections.

that we actually observe part of the unresolved $J^\pi = 0^+$ double-dipole strength.

D. Width of the double-dipole resonance

Figure 6 presents the widths of the double-dipole states observed in the (π^-, π^+) and (π^+, π^-) reactions. In (π^+, π^-) the width of the double dipole is around 10 MeV and is larger than the width of the "single" dipole in (π^+, π^0) [$\langle\Gamma_{GDR}\rangle = 6.3 \pm 1.0$ MeV] by a factor of about 1.5 [15]. This disagrees somewhat with theoretical estimates that the width of the double GDR, as a two-phonon state, should be twice the GDR width [2, 16]. The solid lines are the weighted averages of the data, if the widths in a given mode are independent of A. For (π^+, π^-) the weighted average is $\langle\Gamma_{DD}\rangle = 9.23 \pm 0.76$ MeV and for (π^-, π^+) $\langle\Gamma_{DD}\rangle = 8.60 \pm 0.51$ MeV. In (π^-, π^+) our average widths are about twice the average widths measured for the single dipole in (π^-, π^0) $\langle\Gamma_{GDR}\rangle = 4.2 \pm 1.0$ MeV [15]. The double dipole on ^{27}Al in (π^-, π^+) has a width of only 6.4 ± 1.0 MeV and thus is overestimated by the above constant average. In the (π^-, π^+) reaction the double dipole has only a single isospin component, and therefore is expected to be narrower than in (π^+, π^-) where the observed resonance is composed of two to five isospin components. Table III summarizes the deduced widths of the double-dipole resonances observed in the two DCX modes.

E. Cross-section ratios and background analysis

Figure 7 presents the cross-section ratios for the double-dipole resonances reached in the (π^-, π^+) and

FIG. 7. Ratio of the double-dipole cross sections in (π^-, π^+) to (π^+, π^-) taken from Table III plotted as a function of A. The dashed line is to guide the eye.

(π^+, π^-) reactions on the same target nuclei. For all nuclei with $N > Z$ studied in the present work (^{13}C, ^{27}Al, ^{56}Fe, ^{59}Co, and ^{93}Nb) the cross section in (π^-, π^+) is weaker than in (π^+, π^-). The suppression of the (π^-, π^+) cross sections is nearly independent of atomic mass, but the ratio may decrease slightly with A. The effect of Pauli blocking in changing two protons into two neutrons is expected to increase in neutron-rich nuclei. A similar effect was found for the $1\hbar\omega$ excitation of the GDR in pion single charge exchange [15]. The deduced cross-section ratios $R(GDR^2) = \sigma_{DD}(\pi^-, \pi^+)/\sigma_{DD}(\pi^+, \pi^-)$ are listed in Table III. We will return to the ^{40}Ca case later.

Table IV compares the cross-section ratios from DCX with the cross-section ratios $R(GDR) = \sigma_{GDR}(\pi^-, \pi^0)/\sigma_{GDR}(\pi^+, \pi^0)$ for the "single"-dipole ex-
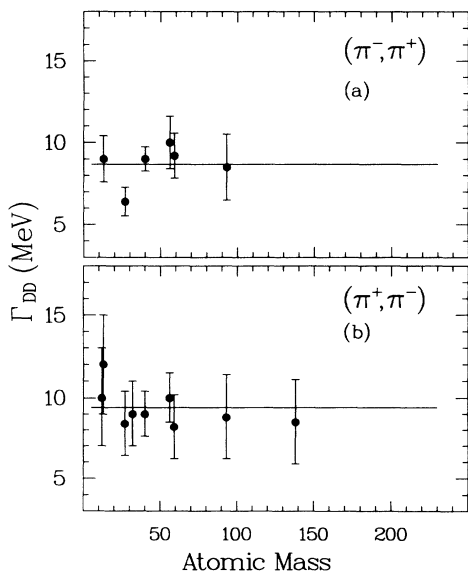

FIG. 6. Widths of the double isovector giant-dipole state as a function of A for both DCX modes. The solid lines in (a) and (b) are least-mean-square values. The widths were obtained using NEWFIT and a Lorentzian line shape for the resonances as illustrated in Figs. 1 and 2.
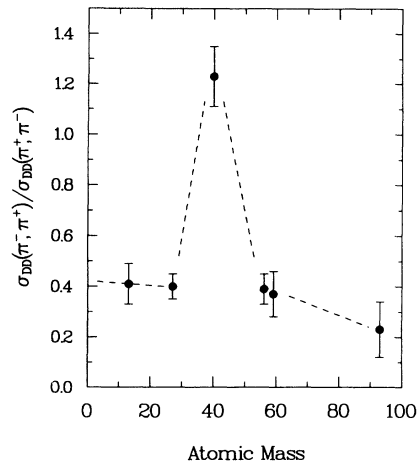
TABLE IV. Comparison between the observed Pauli blocking for the double dipole in DCX, the single dipole in SCX, and theoretical estimates for exciting the isovector giant dipole.

Target	$R(GDR^2)$ [a]	$R(GDR)$ [b]	$R(GDR)_{th}$ [c]
^{13}C	0.41 ± 0.09	–	–
^{27}Al	0.40 ± 0.05	–	–
^{40}Ca	1.23 ± 0.12	1.18 ± 0.24	1.37
^{56}Fe	0.39 ± 0.05	–	–
^{59}Co	0.37 ± 0.09	0.45 ± 0.14	0.45 [d]
^{93}Nb	0.23 ± 0.09	0.43 ± 0.14	0.52 [e]

[a] $R(GDR^2) = \sigma_{DD}(\pi^-, \pi^+)/\sigma_{DD}(\pi^+, \pi^-)$. The double-dipole cross sections are taken from Table III.

[b] $R(GDR) = \sigma_{GDR}(\pi^-, \pi^0)/\sigma_{GDR}(\pi^+, \pi^0)$. GDR peak cross sections from single charge exchange (Ref. [15]). For ^{59}Co and ^{93}Nb we give the ratios measured for ^{60}Ni and ^{90}Zr, respectively.

[c] Reference [17].

[d] Theoretical value for ^{60}Ni (Ref. [17]).

[e] Theoretical value for ^{90}Zr (Ref. [17]).

citation from pion SCX data [15]. Since no data are available for SCX on ^{59}Co and ^{93}Nb, we used in Table IV data for the nearest nuclei (^{60}Ni and ^{90}Zr) for which data are available. Also listed in the table are the theoretical predictions for the cross-section ratios for exciting the GDR in (π^-, π^0) and (π^+, π^0) using transition densities from Hartree-Fock—random-phase-approximation calculations [17]. No theoretical work has been reported for the Pauli-blocking effect in (π^-, π^+) compared with (π^+, π^-) transition strengths. However, the deduced cross-section ratios for the double dipole in DCX from the present study seem to be in good agreement with the SCX data and the theoretical predictions. For example, for nuclei with large neutron excess, one would expect the blocking effect in DCX to be roughly the square of the corresponding attenuation factor in SCX, i.e.,

$$R(\text{GDR}^2) = [R(\text{GDR})]^2, \tag{4}$$

since, in the simplest picture, pion DCX can be viewed as two sequential SCX processes. This estimate seems to be close to the measured cross-section ratio for the double dipole on ^{93}Nb: $R(\text{GDR}^2) = 0.23 \pm 0.09$ in the present study. For lighter nuclei one would expect $R(\text{GDR}^2)$ to be somewhere between $R(\text{GDR})$ and $[R(\text{GDR})]^2$ as observed for ^{59}Co. In the very light nuclei ^{13}C and ^{27}Al the measured cross-section ratio of (π^-, π^+) to (π^+, π^-) is however unexpectedly small.

The nucleus ^{40}Ca is an exceptional case in which the double-dipole cross section in (π^-, π^+) is larger than in (π^+, π^-). This result might be due to the differences in the spatial distributions of the protons and neutrons in the self-conjugate ^{40}Ca nucleus. It is well known that, because of the Coulomb interaction, the protons in ^{40}Ca are expelled relative to the neutrons. In an $N = Z$ nucleus such as ^{40}Ca the Coulomb interaction causes a slight excess of the proton density at the surface of the nucleus. Hartree-Fock calculations, for example, give a root-mean-square radius for the proton distribution $\langle r^2 \rangle_p^{1/2}$ larger by about 1% than the rms radius of the neutron distribution [18]. This slight excess of protons at the surface of ^{40}Ca could cause the (π^-, π^+) cross sections to be larger than the (π^+, π^-) cross sections. A similar increase of the GDR cross section was also observed in (π^-, π^0) compared with (π^+, π^0) in SCX on ^{40}Ca (Table IV); however, in pion DCX the effect seems to be more dramatic—as discussed next in the background analysis.

Figure 8 combines all background spectra from the two DCX modes. The background arises from DCX cross section to the continuum of states encountered in the nucleus at high excitation energies. Some remarkable features are observable in these spectra. For a given A the cross section to the continuum increases with Q value—(most likely) due to the increase in the density of states with increasing excitation energy in the final nucleus. Furthermore, for a given Q value, the background level increases with A, because of the increase in the number of neutrons and protons available for DCX reactions. However, there is a clear irregularity in both Figure 8(a) and Fig. 8(b). In the (π^-, π^+) reaction [Fig. 8(a)] the ^{40}Ca background cross section is the highest,

and has the largest overall DCX cross section of any nucleus up to ^{93}Nb. On the other hand, in the (π^+, π^-) reaction [Fig. 8(b)] ^{40}Ca is again out of order, but now has the smallest background cross section. It seems very likely that this remarkable irregularity arises from the Coulomb polarization effects in the initial and final states as mentioned earlier. Around the (3,3) resonance the pions probe mainly the surface of the nucleus, and therefore DCX is most sensitive to the nuclear tail, amplifying the influence of the Coulomb effects which cause an excess of protons on the nuclear surface of ^{40}Ca [18]. This will enhance the (π^-, π^+) cross section and suppress the (π^+, π^-) cross section on ^{40}Ca as is indeed observed experimentally. This feature is shown more dramatically in Fig. 9 where the background cross section is plotted versus A for different 5-MeV energy bins. Figure 9(a) presents the (π^-, π^+) and Fig. 9(b) the (π^+, π^-) data. The irregularity of the ^{40}Ca case is now more obvious. The cross sections for the different energy bins increase with A except for a local maximum for ^{40}Ca in (π^-, π^+) for all energy bins, and a local minimum in the inverse (π^+, π^-) reaction.

These features seem to be consistent with the available inclusive DCX data on ^{40}Ca and ^{16}O at 240 MeV [19, 20]. The inclusive spectra on ^{40}Ca have a larger overall cross section than on ^{16}O in the (π^-, π^+) reaction,
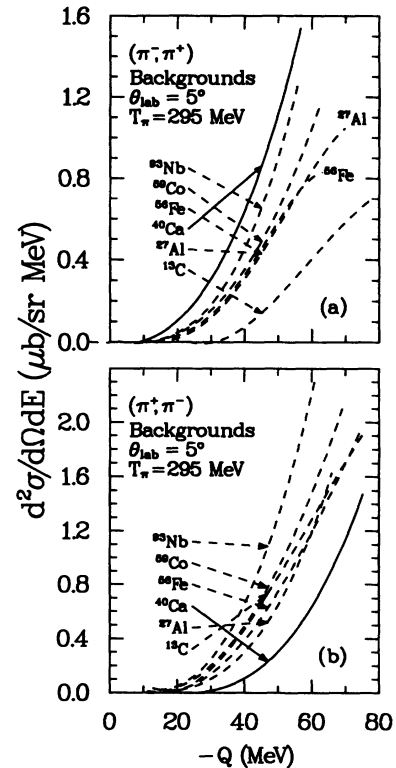

FIG. 8. (a) Fitted background spectra for all targets studied in the (π^-, π^+) reaction in the present work at 5° and $T_\pi = 295$ MeV. The background has been generated using a polynomial shape with use of NEWFIT as shown by the dashed lines in Figs. 1 and 2. (b) Same as (a) but for the inverse (π^+, π^-) reaction studied earlier Ref. [2].
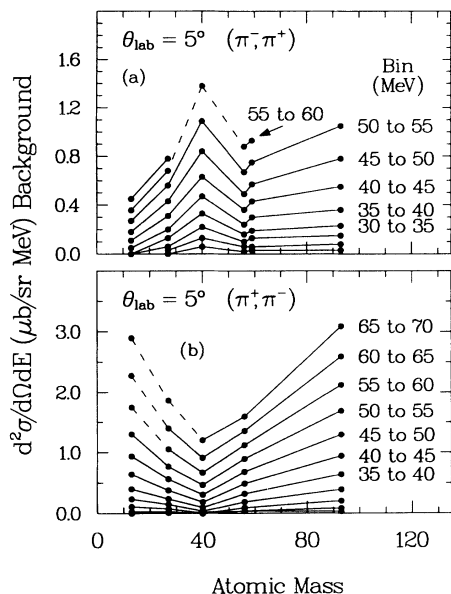
FIG. 9. Doubly differential cross sections of the background spectra from Fig. 8 plotted versus A for different 5-MeV Q-value bins. The data in (a) are from the present study, while those in (b) are from Ref. [2]. The dashed lines at some higher energy bins are extrapolations from the measured spectra.

but have comparable cross sections in the (π^+, π^-) reaction in the Q-value region covered by the present study. These features demonstrate again the overall enhancement of (π^-, π^+) over (π^+, π^-) cross sections on ^{40}Ca. For ^{16}O this effect is found to be much smaller, as would be expected for a light nucleus.

In the above analysis we compared only spectra from the same DCX mode. One can also try to compare spectra from both (π^+, π^-) and (π^-, π^+) reactions on the same target nucleus. For example, Fig. 10 presents such a comparison for the self-conjugate ^{40}Ca nucleus. Figure 10(a) shows the data for (π^+, π^-) and (π^-, π^+) on ^{40}Ca as a function of Q value. The (π^+, π^-) cross sections are substantially lower than the (π^-, π^+) cross sections for given Q values. To understand this phenomenon, we should remember that the same Q value in the two reactions corresponds to very different excitation energies in the final ^{40}Ti and ^{40}Ar nuclei, and thus to different densities of states in these nuclei. (Note that the total Coulomb displacement energy in ^{40}Ti-^{40}Ar is about 28 MeV.) If we correct for this effect by aligning the corresponding ground states (i.e., plotting the cross sections as a function of excitation energy), the two spectra come very close as expected from charge symmetry. This is shown in Fig. 10(b). However, as can be seen from Fig. 10(b), there are still small differences in the two spectra, which should be expected because after all the Coulomb interaction does break charge symmetry to some degree. For example, in the ^{40}Ca target nucleus, as we already mentioned, the protons are slightly expelled with respect to the neutrons. Furthermore, there are kinematical charge symmetry breaking effects, such as
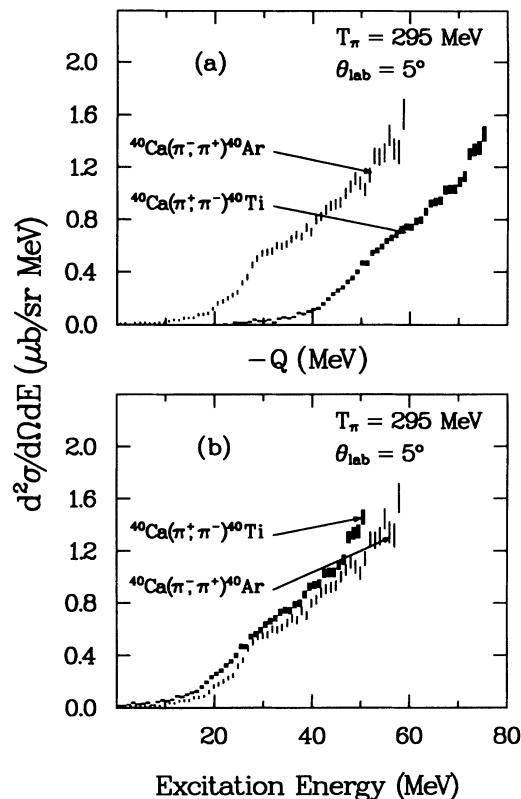

FIG. 10. (a) Comparison between the doubly differential cross-section spectra for the ^{40}Ca$(\pi^-, \pi^+)^{40}$Ar and the ^{40}Ca$(\pi^+, \pi^-)^{40}$Ti reactions at $T_\pi = 295$ MeV and $\theta_{lab} = 5°$ plotted as a function of Q value. The short vertical thin and thick lines represent the statistical uncertainty of the data, respectively. (b) Same as (a) except for plotting the two spectra as a function of excitation energy in the final mirror nuclei.

the dependence of the t matrices on the effective energy of the outgoing projectile, which will produce differences in the two types of reactions. A detailed theoretical study of this effect would be of considerable interest. We are able to make this kind of straightforward comparison in the case of ^{40}Ca in which we are dealing with mirror final nuclei, and there are no contributions from the symmetry energy. Not so are the $N - Z > 0$ target nuclei, where the final nuclei are not charge conjugates and the comparison is more complicated because of the isospin splitting caused in the (π^+, π^-) reactions by the symmetry energy and the differences in the available configuration space for the two DCX modes.

F. Mass dependence of the double dipole

Figure 11 compares present and past data with the results of simple sequential-model calculations using the pion coupled-channel impulse-approximation (CCIA) code NEWCHOP [13]. The cross sections, when divided by $(NZ)^2$, are seen to follow a power law in A, Ref. [2].

The calculations include the ground state (g.s.), the giant-dipole resonance (GDR), and the double dipole (GDR^2). The calculations were normalized by extracting
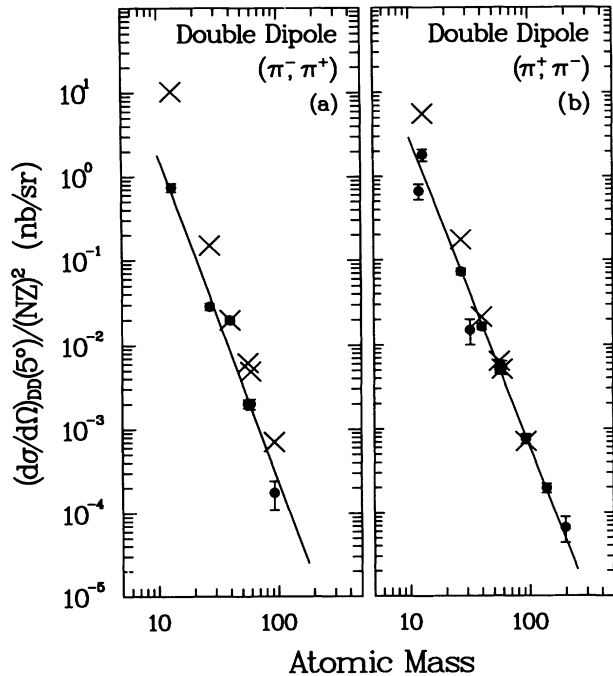
FIG. 11. Plots of the double-dipole cross sections at 5° divided by $(NZ)^2$ vs A for the two DCX modes. The $\times$'s are theoretical calculations as described in the text, and the filled circles are data (a) from the present study and (b) from Refs. [2] and [3]. Both (a) and (b) contain nearly superposed pairs of data points for ^{56}Fe and ^{59}Co. The solid lines are power-law fits to the data. ^{13}C is a light nucleus where the DD does not exhaust the energy weighted sum rule.

β from the energy weighted sum rule in the form [21, 22, 14]

$$\Delta E \left[\int_0^\infty \beta r \rho'(r) r^2 dr \right]^2 = \frac{9}{4\pi} \frac{\hbar^2}{2M} \frac{NZ}{A} e^2. \qquad (5)$$

The values for ΔE were obtained from the following parametrization[23]:

$$\Delta E = 77.9 A^{-1/3} [1 - \exp(-A/238)]$$
$$+ 34.5 A^{-1/6} \exp(-A/238). \qquad (6)$$

Details of the calculations are in Table V.

The data for (π^+, π^-) is from Ref. [2], except for the recent ^{27}Al data point [3]. The nuclei ^{12}C and ^{32}S are deformed and do not follow the power-law fit represented by the solid lines. The data for (π^-, π^+) is from the present work.

TABLE V. Details of the CCIA calculation normalized to the energy weighted sum rule.

Nucleus	ΔE	Matrix element [a]	β
^{13}C	23.06	1.438	0.3860
^{27}Al	20.57	2.200	0.2310
^{40}Ca	19.29	2.774	0.1520
^{56}Fe	18.21	3.372	0.1330
^{59}Co	18.04	3.467	0.1305
^{93}Nb	16.53	4.529	0.0935

[a] This is the integral in Eq. (5).

IV. SUMMARY

The (π^-, π^+) reactions were used to selectively populate the double isovector giant-dipole resonance with a $\Delta T = +2$ nuclear probe. The energy of the double dipole decreases with A in (π^-, π^+) whereas it appears at a constant Q value in the inverse (π^+, π^-) reaction. The double-dipole resonances observed in the present study are closely related via Coulomb energy and isospin symmetry to previous observations of the double dipole in the (π^+, π^-) reactions on the same target nuclei. The cross sections for the double GDR in (π^-, π^+) are suppressed by Pauli-blocking effects and are generally a factor of 2 to 4 weaker (in the region covered by this study) than in (π^+, π^-) on the same target nuclei—with the exception of the self-conjugate ^{40}Ca nucleus. The width of the doubly excited GDR in (π^+, π^-) is about 1.5 times the width of the "single" dipole in (π^+, π^0). In (π^-, π^+), $\Gamma_{DD} \approx 2\Gamma_D(\pi^-, \pi^0)$. A partial angular distribution was measured for the double dipole on ^{40}Ca and found to have predominantly a quadrupole shape, similar to that measured in ^{40}Ca$(\pi^+, \pi^-)^{40}$Ti. The cross sections for the double dipole observed in (π^-, π^+) have a simple mass dependence but with a larger A-dependent attenuation factor than that observed in (π^+, π^-). Background analysis of the continuum DCX cross sections demonstrates the high sensitivity of pion DCX reactions to Coulomb polarization effects.

ACKNOWLEDGMENTS

[1] S. Mordechai et al., Phys. Rev. Lett. 61, 531 (1988).
[2] S. Mordechai et al., Phys. Rev. C 41, 202 (1990).
[3] S. Mordechai et al., Phys. Rev. C 43, R1509 (1991).
[4] H. A. Thiessen et al., Los Alamos Scientific Laboratory Report No. LA-6663-MS, 1977 (unpublished); S. J. Greene et al., Phys. Lett. 88B, 62 (1979).
[5] C. L. Morris, J. F. Amann, R. L. Boudrie, N. Tanaka, S. J. Seestrom-Morris, L. C. Bland, P. A. Seidl, R. Kiziah, and Steven J. Greene, Nucl. Instrum. Methods A 238, 94 (1985).
[6] G. Rowe, M. Salomon, and R. H. Landau, Phys. Rev. C 18, 584 (1978).
[7] S. Mordechai et al., Phys. Rev. C 40, 850 (1989).
[8] S. Mordechai et al., Phys. Rev. C 43, 1111 (1991).

[9] C. L. Morris (unpublished).

[10] J. M. O'Donnell and H. T. Fortune, Phys. Rev. C **44**, 1481 (1991).

[11] M. S. Antony, J. Britz, and A. Pape, At. Data Nucl. Data Tables **40**, 9 (1988).

[12] D. Zubanov, R. A. Sutton, M. N. Thompson, and J. W. Jury, Phys. Rev. C **27**, 1957 (1983).

[13] E. Rost, computer code CHOPIN (unpublished). The code has been modified by one of us (C.L.M.) to calculate pion charge-exchange reactions and renamed NEWCHOP.

[14] J. M. O'Donnell, H. T. Fortune, and E. Rost, Phys. Rev. C **44**, 2426 (1991).

[15] A. Erell, J. Alster, J. Lichtenstadt, M. A. Moinester, J. D. Bowman, M. D. Cooper, F. Irom, H. S. Matis, E. Piasetzky, and U. Sennhauser, Phys. Rev. C **34**, 1822 (1986).

[16] N. Auerbach, Ann. Phys. **197**, 376 (1990).

[17] N. Auerbach and Amir Klein, Phys. Rev. C **28**, 2075 (1983).

[18] N. Auerbach, Phys. Rev. Lett. **49**, 913 (1982).

[19] S. A. Wood, Los Alamos National Laboratory Report No. LA-9932-T, 1984 (unpublished).

[20] J. L. Matthews, *Proceedings of the LAMPF Workshop on Pion Double Charge Exchange* [Los Alamos National Laboratory Report No. LA-10550-C, 1985 (unpublished)].

[21] A. Bohr and B. Mottelson, *Nuclear Physics* (Benjamin, New York, 1975), Vol. II.

[22] A. Gal, Phys. Rev. C **25**, 2680 (1982).

[23] B. L. Berman and S. C. Fultz, Rev. Mod. Phys. **47**, 713 (1975).

[24] A. H. Wapstra, G. Audi, and R. Hoekstra, At. Data Nucl. Data Tables **39**, 281 (1988).